Received: 2 June 2022 | Revised: 11 August 2022 | Accepted: 15 August 2022

DOI: 10.1002/aic.17902

RESEARCH ARTICLE

Separations: Materials, Devices and Processes

AIChE JOURNAL

# Development of enhanced three-dimensional printed packings for scale-up of distillation columns: A successful case study

Johannes Neukäufer[1] | Mohamed Adel Ashour[1] | Nadin Sarajlic[2] | Harald Klein[2] | Sebastian Rehfeldt[2] | Heiko Hallmann[3] | Sebastian Meinicke[3] | Jürgen Paschold[3] | Carsten Knösche[3] | Thomas Grützner[1]

[1]Laboratory of Thermal Process Engineering, Institute of Chemical Engineering, Ulm University, Ulm, Germany

[2]Institute of Plant and Process Technology, Department of Energy and Process Engineering, TUM School of Engineering and Design, Technical University of Munich, Garching, Germany

[3]BASF SE, Ludwigshafen am Rhein, Germany

**Correspondence**
Johannes Neukäufer, Laboratory of Thermal Process Engineering, Institute of Chemical Engineering, Ulm University, Albert-Einstein-Allee 47, 89081 Ulm, Germany.
Email: johannes.neukaeufer@uni-ulm.de

## Abstract

This publication presents a general approach for the enhancement of packings regarding scalability, separation efficiency, and fluid dynamic properties using three-dimensional (3D) printing. The methodology is used to develop miniaturized, scalable packings for process development, and scale-up applications. For this purpose, a 3D printable computer-aided design version of the Rombopak 9M industrial packing (RP9M-3D), which is known for its positive scalability properties, was created. An initial characterization by means of computational fluid dynamics simulations and mass transfer measurements reveals positive but also negative design properties. These findings are used to create a more advanced, miniaturized packing structure, the XW-Pak. The evolved structure is compared to the RP9M-3D. The simulation and experimental results show that the enhanced packing, which is still in the early stages of development, exhibits higher separation efficiencies with improved scalability properties at the same void fraction and surface area than the RP9M-3D.

**KEYWORDS**
3D printing, distillation, miniaturization, scale-up, structured packing

## 1 | INTRODUCTION

In the chemical industry, the thermal separation processes of distillation, absorption, and desorption are often realized in packed columns. To maximize the efficiency of these apparatuses, 3D printing is increasingly utilized to develop new packings with higher capacity, greater separation efficiency, and lower pressure drop. However, most applications are still limited to laboratory and pilot plant scales.

Rotating packed beds can also be used for the separation of mixtures, for which innovative packings are developed, designed, and characterized. Gładyszewski et al.[1] present a proof of concept for using additive manufacturing to create tailored packings for these devices. Wen et al.[2] characterize additively manufactured wire mesh packings for use in rotating packed beds and Qammar et al.[3] show an experimental approach for the development of 3D printed rotating packed bed packings for distillation. The development of 3D printed packings for standard vertical packed columns for absorption, desorption, and distillation processes are becoming increasingly attractive. Bara et al.[4] develop random packings for laboratory-scale columns. Bolton et al.,[5] Miramontes et al.,[6] and Xiao et al.[7] design additively manufactured packings for carbon capture applications. Grinschek et al.[8] present regular microstructured 3D printed elements for the intensification of gas–liquid contactors, especially for $CO_2$-absorption. At the University of Toulouse, a wire-based 3D printable packing is

developed and characterized for use in gas/liquid contactors.[9] Zimmer et al.[10] present triple-periodic minimal surface packings that are manufactured via 3D printing. At the Ruhr University Bochum, replica of the Raschig Super Pak 350Y and a grid structured packing are created and 3D printed with an enclosing column wall. Reitze et al.[11] examine the liquid distribution and Riese et al.[12] conduct experiments for further characterization of these packings. The aforementioned publications predominantly focus on gas-liquid contactors. Only a few publications specifically address distillation. Mardani et al.[13] illustrate the first 3D printed hexagonal packed column for distillation and Grinschek et al.[14] present a compact distillation device by considering the method characteristics of additive manufacturing.

Within this publication, distillation represents a particularly important role as it is the most important and energy-intensive thermal separation process.[15] The joint research project of Ulm University, the Technical University of Munich, and BASF SE focuses on the creation of miniaturized scalable packings for process development and scale-up of distillation columns using 3D printing. Important packing characteristics are great flexibility to gas and liquid throughputs with an overall high capacity combined with a high, almost constant separation efficiency.[16] Within this work, the term scalability is defined as a constant and reproducible separation efficiency, which is independent of the gas load.

For the state-of-the-art implementation of industrial-scale columns, preliminary tests in laboratory-scale columns are indispensable in many cases. Especially complex separations with new or unknown chemicals require experimental validations. In this course, up to 2000 new chemicals are commercialized annually.[17–19]

There are several approaches for scaling up packed columns, for example, according to Houfton et al.,[20] whereof the most common approach is to use calibrated test columns in a laboratory scale.[21] These columns are operated with a suitable standard test mixture[22] such as *n*-heptane/cyclohexane, chlorobenzene/ethylbenzene, or *o*-/*p*-xylene.

The scale-up procedure is as follows. First, the separation efficiency of the calibrated test column is determined using the standard test mixture. Furthermore, data in columns with significantly larger diameters ($d_C \geq 400$ mm) are available for these standard test mixtures, from external sources like vendor information, the Fractionation Research Inc. (FRI), or the Separations Research Program (SRP). Based on this, correlations for the transferability of the results from the laboratory to pilot plant or industrial scale can be derived. Second, the required laboratory column height for the actual mixture is determined. For this purpose, the mixture is separated in the calibrated test column and the packed height is varied until the desired product specifications are met. Third, the column height at the laboratory scale is translated to the desired pilot or industrial scale. These measurement data from the first and second steps are used in conjunction with appropriate models, empirical approaches, or estimated values for the scale-up process.[21] In order to guarantee the feasibility of this approach, the packing should possess a separation efficiency which is independent of the *F*-factor. Furthermore, the measurements should be reproducible and of high accuracy. Then, even the use of different packing types and materials in the laboratory- and the industrial-scale column is possible while maintaining scalability.[21]

However, according to literature using pilot scale equipment with column diameters between 150 and 200 mm instead of laboratory scale columns for the above-mentioned scale-up process would be the most reliable approach.[23] Nevertheless, the time and costs for scaling up by apparatuses of this dimension are disproportionately large. Moreover, sufficient amounts of chemicals are often not available. Thus, to make this procedure more time and cost-efficient, smaller column diameters are desired. Consequently, these are usually reduced to approximately 50 mm to generate packing-specific experimental data.[23] Here, the accuracy requirements of test columns can still be met, while the scale-up with column diameters of $d_C \approx 30$ mm are discussed controversially.

However, a further decrease would be of great advantage if scalability and the accuracy of the measurements could be maintained. The potential cost savings for preliminary experiments in a laboratory or pilot plant scale are very high due to several factors. The miniaturized diameter reduces the throughput in the column and, thereby, the size and costs of the column components. This decreases the need for costly fume hood areas. The requirement for expensive chemicals, which are often produced in complex multi-stage synthesis steps, is reduced to a minimum due to a smaller volume of liquid in the system and lower throughputs. In addition, the safety requirements and associated costs are significantly reduced. However, as a result of the miniaturization, an increased wall-to-core ratio intensifies effects such as liquid wall flow and condensation due to heat loss at the column wall.

Consequently, to enhance the scalability of miniaturized test columns, on the one hand, the heat losses via the column wall must be minimized. On the other hand, packings with a high separation efficiency independent of the *F*-factor lead to a simpler and thus improved transferability of measurement results for scale-up.

Within the research project, a scalable distillation column with the target diameter of 20 mm is produced using additive manufacturing. Based on a design methodology discussed in detail elsewhere,[24] an approach for the development of improved packing structures in laboratory or pilot plant scale is presented. Subsequently, the first development steps for the enhancement of innovative packing structures will be demonstrated. Proof of the approach's viability is confirmed with mass transfer measurements in a distillation test rig for characterizing additively manufactured, miniaturized packings at the Ulm University.[25] Accordingly, this paper acts as a proof of concept of this methodology.

Further optimization cycles have already been carried out successfully but are not the content of this publication. The presented concept is not limited to the objects defined here and could be applied to other problems, such as maximizing the packing capacity for absorption applications or designing other column internals like liquid collectors for dividing wall columns. However, the methodology presented below is predominantly described using the example of enhanced packing structures for scale-up applications.

## 2 | METHODOLOGY FOR THE DEVELOPMENT AND ENHANCEMENT OF MINIATURIZED PACKINGS

Figure 1 shows the general approach to the development of enhanced, miniaturized packings with improved scalability and reproducibility properties. In the beginning, an initial packing structure must be available, which is generated with a suitable computer-aided design (CAD) program (Section 2.1), such as Autodesk Inventor® (Design). The structure is then characterized by means of computational fluid dynamics (CFD) simulations which are presented in Section 2.2. The CFD simulations are divided into two areas. On the one hand, single-phase gas flow simulations are used to determine the specific dry pressure drop and mass transfer coefficients. On the other hand, two-phase flow simulations are used to examine the liquid distribution in the packing structures. Insights from the simulation results can be used to eliminate weak points or highlight advantageous properties of the packing structure at an early stage of the development process. These issues will be discussed in more detail in the course of this article (Section 3). The close interaction of design and CFD simulation represents a first iteration loop. Promising structures derived in the process are 3D printed and investigated in an experimental test rig to determine the separation efficiency. Suitable evaluation criteria are, for example, a homogeneous liquid distribution and low liquid wall flow, or good mixing of the gas and liquid phases. At the same time, high mass transfer coefficients and low-pressure drops are desirable. While 3D printing is already considered in Section 2.1, the necessary experimental investigations are described in Section 2.3. Based on the new findings from mass transfer measurements, the packing structure resulting from the first iteration loop is modified. Modifications can either be a simple variation of the dimensioning parameters or a transformation towards a new design of the packing structure. This results in iteration loop 2. The process of running through both iteration loops is repeated until a packing is obtained that meets the desired requirements. Additional improvement cycles or the use of other initial structures as input to this methodology can lead to even better packings.

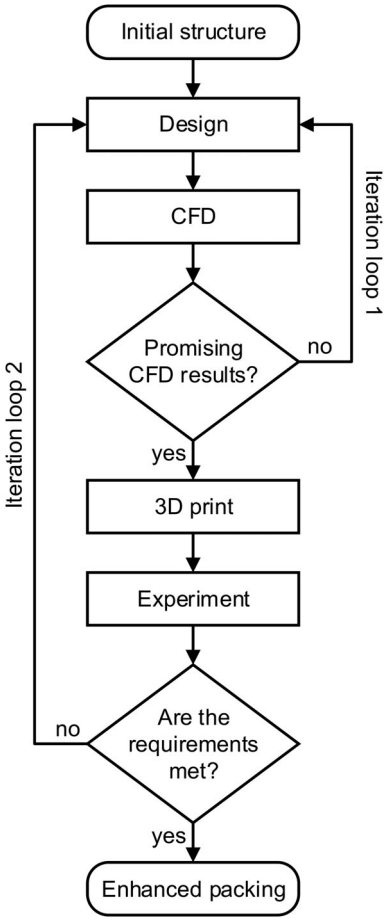


**FIGURE 1** Procedure for the development of improved packing structures for the scale-up of distillation columns

### 2.1 | Design and additive manufacturing

The components for 3D printing are created in the CAD software Autodesk Inventor® via the Visual Basic for Applications (VBA) interface. With this approach and by using parameterized geometries, the CAD components can be modified or created within seconds.[24] The components needed for the implementation in a distillation column were 3D printed externally at the company Blue Production GmbH & Co. KG. The selective laser sintering (SLS) 3D printer EOS P 396 was used with the material polyamide 12 (PA12). The layer thickness during the print was 120 µm. The components were washed and infiltrated after 3D printing. PA12 was preferred over metallic materials for the studies because it is inexpensive and its chemical and temperature resistance to the substances used in this work is sufficient. However, metal packings are more relevant for industrial applications. This approach is justified because stainless steel packings show predominantly better results than PA12 packings. Investigations regarding packing wetting and separation efficiency measurements have confirmed such a behavior and show that the approach is conservative. More detailed information is provided in a previous publication.[25] A tongue and groove system allows the packing segments to be accurately stacked on top of each other, without being compressed or deformed when inserting them into the column (Figure S1). To ensure that the packings fit precisely into the column jacket, the manufacturing tolerances should be coordinated with the manufacturer or successively adjusted. The tolerances of the additively manufactured parts depend on the 3D printer and its specifications.

The former industrial Rombopak 9M packing, which is characterized by good scalability properties, is used as the initial structure for the methodology described in Section 2. To apply this methodology, a 3D printable version of the Rombopak 9M from Kühni/Sulzer[26] was created, hereafter referred to as RP9M-3D. This structure with all relevant dimensioning parameters has already been described in a previous publication.[25] When reducing the diameter of the packings from DN50 to DN20, the cross-sectional area is reduced by a factor of

| Packing | RP9M-3D | | XW-Pak | |
|---|---|---|---|---|
| Diameter | DN50 | DN20 | DN50 | DN20 |
| Void fraction $\varepsilon$ in % | 88 | 88 | 89 | 89 |
| Specific geometric surface area $a_{geo,P}$ of the packing in $m^2m^{-3}$ | 359 | 355 | 349 | 351 |
| Specific geometric surface area $a_{geo,PW}$ of the packing with column wall in $m^2m^{-3}$ | 430 | 531 | 420 | 529 |

**TABLE 1** DN50 and DN20 packing parameters of the RP9M-3D and an enhance packing structure XW-Pak

6.25. For illustration, a CAD model of a packing segment at DN50 and DN20 is shown in Figure S1.

Table 1 lists the values of the void fraction $\varepsilon$ and the specific geometric surface area $a_{geo}$ of RP9M-3D. Since the column wall significantly contributes to the specific geometric surface area in laboratory scale packed columns, values are given for the packing without $a_{geo,P}$ and with the column wall $a_{geo,PW}$.

## 2.2 | CFD simulations

To gain further insight into the fluid dynamic behavior of the considered packings, CFD simulations are performed in OpenFOAM® Version v2006. This leads to large time and costs savings during the development process since unfavorable packing characteristics can be detected at an early stage and only promising structures are investigated experimentally. For the simulative characterization of the packings, single-phase gas flow and two-phase flow simulations of the irrigation behavior, which are described in Sections 2.2.1 and 2.2.2, are used.

### 2.2.1 | Single-phase gas flow simulation

The steady-state, incompressible single-phase gas flow simulations are conducted using the *simpleFoam* solver. In the following, the basic principle of the simulation is given, since a detailed description would go beyond the scope of this publication. The gas flow is described by solving the continuity and the momentum equation given in Equations (1) and (2).[27] Here, $\vec{u}$ represents the velocity vector, $p$ the pressure, $\rho$ the density, and $\nu$ and $\nu_t$ the molecular and turbulent kinematic viscosities. The acceleration due to gravity is neglected within the single-phase gas flow simulations.

$$\nabla \cdot \vec{u} = 0 \tag{1}$$

$$\vec{u} \cdot \nabla \vec{u} = -\nabla p \cdot \frac{1}{\rho} + \nabla\left((\nu + \nu_t) \cdot \nabla \vec{u}\right) \tag{2}$$

The setup of the single-phase gas flow simulations is characterized by a cylindrical tube consisting of three sections. The upper and lower sections of the computational domain are designed as empty tubes. The packing structure, which is to be characterized by the CFD simulations, is located in between (Figure S2). During the simulation, nitrogen flows into the calculation domain from the bottom inlet with the superficial gas velocity $u_G = 0.9327\ ms^{-1}$. This corresponds to an *F*-factor of $F = 1.0\ Pa^{0.5}$. Nitrogen is often used for dry pressure drop measurements, so classification and comparison with other packings are simplified. The fluid properties of nitrogen used for the calculation were taken from the VDI heat atlas for a temperature of $T = 20°C$ and a pressure of $p = 1.0$ bar.[28]

Within the single-phase gas flow simulations, residuals $< 10^{-5}$ were assumed as the convergence criterion. Furthermore, relatively low Reynolds numbers (Re < 2300) are found, indicating a laminar regime. However, since the turbulence behavior in porous media, such as packing structures, is discussed in many different ways,[29] the $k-\omega$ SST turbulence model for low-Reynolds turbulent flows was identified as a suitable option.[30] Moreover, laminar comparative simulations did not show any significant differences.

*Calculation of the specific dry pressure drop*

Once convergence is reached in the simulations, the specific dry pressure drop is calculated by the slope of the linear regression of the pressure along the packing. For this purpose, several equidistant horizontal evaluation planes are introduced to determine the area-weighted pressure at the upper and lower limit and inside the packing. At this point, it must be mentioned that the detailed scientifically correct validation is still pending. However, previous packings were examined for plausibility using experimental measurement data from BASF. Furthermore, the simulations were compared in different CFD tools and checked for consistency (OpenFOAM − StarCCM+). Additionally, the distillation test rig at Ulm University (Section 2.3) is currently being upgraded so that reliable experimental specific dry pressure drop measurements can be conducted and compared to the simulation results.

*Calculation of mass transfer coefficients*

Many approaches exist for the study of mass transfer. The analogy of heat and mass transfer is often used as a simplified approach.[31] Another method that has proven to be very fast, easy to implement, and robust is the use of passive scalars.[27] Within this work, the latter approach is used to determine (volumetric) mass transfer coefficients $\beta$ and $\beta \cdot a_{geo,PW}$.

The absolute values of the mass transfer coefficients depend on the material properties of the real substance system. However, the nitrogen gas utilized in the single-phase simulations is considered as a

model fluid from the standpoint of mass transfer. Consequently, the mass transfer evaluations do not provide exact absolute values but allow a relative comparison of different packing structures at different column configurations. A passive scalar is transported through the calculation domain by convection and diffusion but does not influence the fluid dynamics. It can be considered as a tracer or a concentration $c$. The passive scalar transport equation is shown in Equation (3).[27]

$$\vec{u} \cdot \nabla c = \nabla((D + D_t) \cdot \nabla c) \tag{3}$$

For the single-phase gas flow simulations, an input concentration of $c_{in} = 100\ \mathrm{mol/m^3}$ and a fixed concentration on the packing surface and the packing surrounding wall $c_{PW} = 1\ \mathrm{mol/m^3}$ are defined. Consequently, the latter acts as an infinite sink. These values can be chosen freely as they do not influence the final value of the mass transfer coefficient $\beta$. The molecular diffusion coefficient influences the absolute values of the resulting mass transfer coefficient. However, as long as the same value is used for different simulations, packings can be compared with each other. For the molecular diffusion coefficient of the considered model fluid, the gas-side diffusion coefficient was calculated for an *n*-heptane/cyclohexane mixture at $p = 1$ bar and an average column or boiling temperature of the mixture of $T = 90^\circ\mathrm{C}$ was used,[32] leading to a value of $D = 3.72 \times 10^{-6}\ \mathrm{m^2\ s^{-1}}$. *n*-Heptane/cyclohexane is a standard test mixture for distillation,[22] which is also used for mass transfer measurements within this work (Section 2.3). To estimate the turbulent diffusion coefficient, the relation of the turbulent Schmidt number $Sc_t = \nu_t / D_t$ can be used.[27] According to Tominaga and Stathopoulos,[33] the empirical turbulent Schmidt number ranges from 0.2 to 1.3 for various applications. The value was set to 0.7 in the single-phase gas flow simulations presented here.[34]

The average mass transfer coefficient $\beta$ can be determined according to Equations (4) and (5).[35] The difference between incoming and outgoing molar flows $\dot{N}_{in}$ and $\dot{N}_{out}$ corresponds to the molar flow that has passed to the packing and the surrounding wall $\dot{N}_{PW}$.

$$\dot{N}_{in} - \dot{N}_{out} = \dot{N}_{PW} \tag{4}$$

$$\beta = \frac{\dot{V}}{A_{geo,PW}} \cdot \ln \frac{c_{PW} - c_{in}}{c_{PW} - c_{out}} \tag{5}$$

The approach gives only qualitatively correct results, since the liquid side mass transfer resistance is neglected. However, embedded in the methodology described in Figure 1, this approach allows a fast prediction regarding the mass transfer behavior when comparing different packings. Such a simulation approach assumes that the whole packing surface and the packing-enveloping wall of the height $H_P$ participate in the mass transfer between gas and liquid phases, corresponding to full wetting. However, this is not the case in reality, as the irrigation simulations will prove (Sections 3.1.2 and 3.3.2). In addition, an infinitely thin film thickness of the liquid phase is assumed, so that the gas flow is not affected. This is true to a first approximation since laboratory scale distillation columns usually operate at low *F*-factors $F < 1.0\ \mathrm{Pa^{0.5}}$. Since perfect wetting of the packing cannot be fulfilled in most cases, the results should be further interpreted together with the results of the two-phase flow simulation of the irrigation behavior described in Section 2.2.2.

### 2.2.2 | Two-phase flow simulation of the irrigation behavior

The two-phase flow simulations of the irrigation behavior were developed at the Technical University of Munich in close cooperation with Ulm University. OpenFOAM® v2006 is utilized and the *interFoam* solver has been modified in a way that cyclic boundary conditions can be used at the top and bottom of the cylindrical calculation domain. For this purpose, minor adjustments were conducted for the transfer of the originally used OpenFOAM® Version v1906 of Sarajlic et al.[36] to the v2006 Version. The behavior of the phase interface is modeled by specifying contact angles and using the volume of fluid method. A high resolution in the area of the phase interface plays a decisive role. Mesh dependence studies were carried out for this purpose. Detailed information can be obtained in the publication of Sarajlic et al.[36] At this point, it must be emphasized that considering the different wetting properties of additively and conventionally manufactured materials is beyond the scope of this publication.

The objective of these simulations, in combination with the single-phase gas flow simulations, is to allow a direct comparison between packing structures with respect to the separation efficiency at an early stage of development. Due to uncertainties in contact angles on 3D printed materials[37] and blurred resolution of the phase interface due to the volume of fluid method, the results of the two-phase flow simulations are interpreted qualitatively. The basic setup is shown in Figure 2. Similar to a packed column, a cylindrical calculation domain is selected. This contains the smallest possible repetition unit of a packing segment with the target diameter of $d_P = 20$ mm. Simulations at $d_P = 50$ mm are not performed because the computational effort becomes disproportionately large. The liquid used is *n*-heptane, since the experimental test rig is operated with this chemical.

The gas phase is represented by air. Necessary fluid properties of *n*-heptane and air are related to a temperature of $T = 20^\circ\mathrm{C}$ and a pressure of $p = 1.0$ bar.[36] Initially, a predefined liquid holdup is set that is accelerated by gravitation leading to an overall liquid load, once quasi-steady-state conditions, as illustrated in Figure 2, are reached. By using cyclic boundary conditions at the top and bottom of the calculation domain, the liquid flowing out at the bottom is reentering at the top. In illustrative terms, this means that the simulation duration correlates with the simulated packing height. However, it is important that a quasi-steady state is established, which results from a balance of gravitational and frictional forces. This allows the simulation of a section of a tall column in a vertically centered position. Depending on the initialized holdup of the liquid, a certain liquid distribution establishes inside the packing.

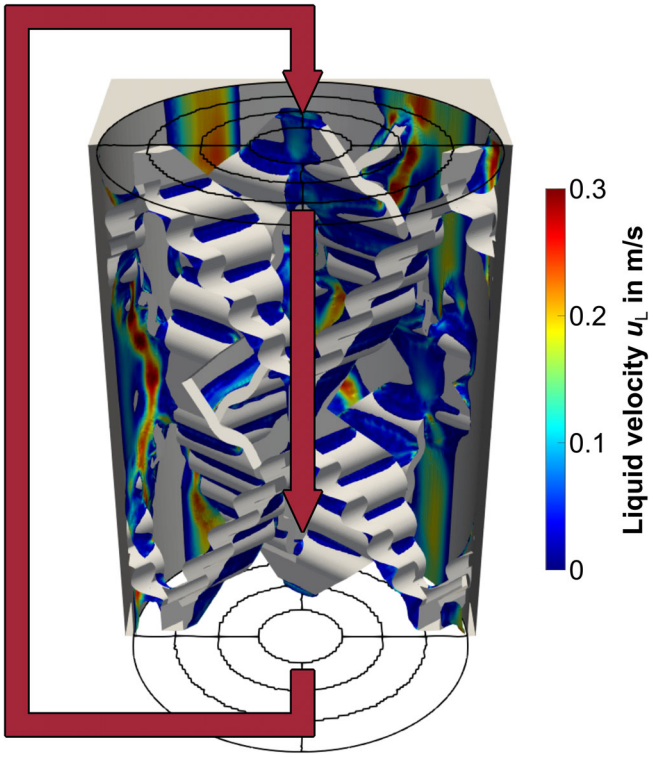


**FIGURE 2** Two-phase flow simulation of the irrigation behavior, illustrated as vertical cut of the calculation domain

The upper and lower end of the domain are segmented into 13 parts, which enables an evaluation of the local liquid load distribution over time. This also allows for an estimation of whether the liquid flow has reached a quasi-steady-state.

Considering the small dimensional scale of miniaturized packed columns at $d_C \approx 20$ mm, it is unavoidable to have unevenly distributed packing geometric pieces, hereafter referred to as crosspieces, over the bottom segmentation shown in Figure 2. Additionally, the column wall effects are significantly influential as shown in Sections 3.1.2 and 3.3.2. In pilot or industrial columns, the large geometric scale allows for a better distribution on average of the packing crosspieces over the bottom segmentation. Consequently, the evaluation of liquid distribution on the discussed miniaturized scale cannot be performed using only local liquid loads since they can be misleading. In order to take these aspects into account, a method was developed together with the Technical University of Munich, considering the arrangement of the packing geometry at the bottom of the computational domain. Within this publication, however, only the liquid distribution spectrum is discussed. A more detailed analysis of the aforementioned new evaluation method can be found in a previous publication by Sarajlic et al.[36]

## 2.3 | Mass transfer measurements

To verify the findings from the CFD simulations, the promising packings resulting from iteration loop 1 (Figure 1) are characterized experimentally. For this purpose, a distillation test rig operated at total reflux is used to determine the separation efficiency and its dependence on the *F*-factor. As mentioned in Section 1, a constant separation efficiency is desired for scale-up applications. The test rig, which was specially created to characterize additively manufactured packings, features a particularly wide operating range with gas loads between $F = 0.1$ Pa$^{0.5}$ and 1.0 Pa$^{0.5}$ for column diameters 20 mm $\leq d_C \leq$ 50 mm. The distillation plant is operated with the standard test mixture *n*-heptane/cyclohexane. Due to the dependency of the height equivalent to a theoretical plate (*HETP*) on the stripping factor $\lambda$, different measurements of different packings at different concentration ranges cannot be adequately compared.[38] The use of the height of a transfer unit ($HTU_{OG}$) solves this problem as it is independent of the considered concentration range and the stripping factor. The $HTU_{OG}$-value is calculated according to Equation (6) assuming a constant relative volatility $\alpha_{12}$, constant internal molar flows and constant values for the heat of evaporation $\Delta h_V$ under total reflux conditions.[16] Here, $\alpha_{avg}$ represents the average relative volatility in the column. $x_1$ expresses the low-boiling molar fraction (cyclohexane) above (T) and below (B) the packing.

$$HTU_{OG} = \frac{H_P}{\frac{1}{\alpha_{avg}-1}\ln\left(\frac{1-x_1^B}{1-x_1^T}\cdot\frac{x_1^T}{x_1^B}\right)+\ln\left(\frac{1-x_1^B}{1-x_1^T}\right)} \quad (6)$$

Detailed information about the (uncertainty) analysis as well as the test rig design and operation are given in a previous publication[25] and in the Supporting Information.

## 3 | RESULTS AND DISCUSSION

In this section, a first enhancement cycle of the methodology described in Section 2 is applied to the RP9M-3D (Section 2.1) as the initial structure. The aim is to develop a packing with improved properties in terms of separation efficiency, scalability (constant $HTU_{OG}$-values), and reproducibility. These properties should be maintained in a typical laboratory operating range between $F = 0.1$ Pa$^{0.5}$ and 1.0 Pa$^{0.5}$, while the specific dry pressure drop $\Delta p_d/H_P$ remains below the maximum value of 2 mbar/m. The initial structure RP9M-3D is first characterized using the CFD simulations described in Section 2.2. Additionally, mass transfer measurements are conducted to allow the comparison of the enhanced packings with the initial structure later on. Based on the RP9M-3D results presented in Section 3.1, the corresponding advantages and disadvantages of the packing are discussed. This provides the basis for the development of a new packing structure, which is presented in Section 3.2. In addition, the new packing structure is characterized by means of CFD simulations and experiments as described in Section 3.3. Furthermore, a direct comparison is made in this respect with the initial structure at DN50 and DN20. It must be emphasized that DN50 is the industry standard for scale-up and DN20 is the target column diameter defined for this work.

### 3.1 | Characterization of the initial structure RP9M-3D

The 3D printable version of the RP9M (RP9M-3D) is described in more detail in a previous publication.[25] The difference to the conventional Rombopak 9M is primarily the significantly greater crosspiece thickness, which results from the use of SLS in the manufacturing process. Furthermore, the crosspiece width was increased and wall wipers were not considered for the time being. Positive and negative packing characteristic features are identified based on the results of the single-phase gas flow simulation and the two-phase flow simulation of the irrigation behavior in Sections 3.1.1 and 3.1.2. Then, the packing structures are investigated with respect to their separation efficiency in the experimental test rig described in Section 3.1.3.

#### 3.1.1 | Single-phase gas flow simulation

Using the single-phase gas flow simulations described in Section 2.2.1, the specific dry pressure drop $\Delta p_d/H_P$ is quantified. In addition, (volumetric) mass transfer coefficients $\beta$ and $\beta \cdot a_{geo,PW}$ are determined to allow the comparison with other packing structures. The results of the single-phase gas flow simulations are listed in Table 2. The specific geometric surface areas with and without consideration of the column wall $a_{geo,P}$ and $a_{geo,PW}$ can be found in Table 1. When the diameter is reduced from DN50 to DN20, the pressure drop increases by 12.6%. This is the result of a significantly higher specific surface area $a_{geo,PW}$ and thus, higher flow resistance.

These effects do not lead to significantly different mass transfer coefficient $\beta$, since the mass transfer behavior inside the packing and at the column wall is similar. Minor differences depend on the packing structure and can result from deviating flow characteristics when comparing the packing structure and the column wall. Here, it is important to note that the mass transfer coefficient is a value averaged over the entire packing with column wall.

In order to estimate the separation efficiency of a packing structure in the form of the $HTU_{OG}$-value, the volumetric mass transfer coefficient $\beta \cdot a_{geo,PW}$ is primarily relevant. When determining the product $\beta \cdot a_{geo,PW}$, the values for the DN20 column are 19.0% higher than those of the DN50 column. This is mainly caused by the additional surface area of the wall available for mass transfer at miniaturized column diameters.[39]

As described in Section 2.2.1, only the mass transfer with the assumption of a fully wetted packing structure and column wall surface is captured by the single-phase gas flow simulations. Two-phase flow simulations are performed to increase the validity of derived trends from the single-phase gas flow simulations by considering the liquid distribution.

#### 3.1.2 | Two-phase flow simulation of the irrigation behavior

By combining the findings from the single-phase gas flow simulations with consideration of the distribution and wetting of the liquid phase, a comprehensive characterization of the packings can be made. This in turn leads to a sound understanding of the fluid dynamics in the considered packing structures. The characterization of RP9M-3D was presented in a previous publication.[36] Additionally, the liquid distribution is illustrated in Figure 3 for an overall liquid load of $B = 7.5\ m^3\ m^{-2}\ h^{-1}$.

Figure 3 shows that the RP9M-3D has very pronounced wall flow at DN20. The liquid flow is significantly reduced in the center of the packing. All in all, a rather poor liquid distribution can be observed within this packing. Based on the uneven liquid distribution, the fundamental potential for improvement of the structure becomes apparent. Since the RP9M-3D is the initial structure, more precise conclusions (Section 3.2) can only be drawn after consideration of the experimental investigations, which will be presented in Section 3.1.3.

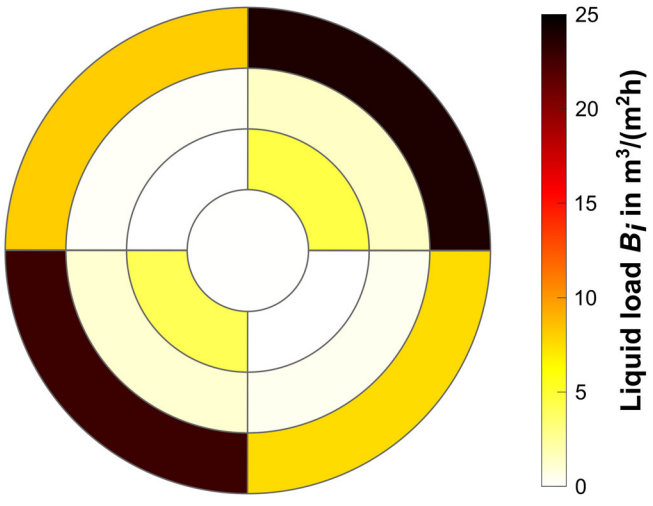


**FIGURE 3** Simulated liquid distribution at the domain ends of the RP9M-3D with an overall liquid load of $B = 7.5\ m^3\ m^{-2}\ h^{-1}$ at DN20 (according to Sarajlic et al.[36])

**TABLE 2** Single-phase gas flow simulation results for the RP9M-3D and the XW-Pak for diameters DN50 and DN20 with consideration of the column wall

| Packing | RP9M-3D | | XW-Pak | |
|---|---|---|---|---|
| Diameter | DN50 | DN20 | DN50 | DN20 |
| Specific dry pressure drop $\Delta p_d/H_P$ in $mbar\,m^{-1}$ | 0.722 | 0.813 | 1.176 | 1.291 |
| Mass transfer coefficient $\beta$ in $mm\,s^{-1}$ | 15.77 | 15.25 | 21.31 | 20.55 |
| Volumetric mass transfer coefficient $\beta \cdot a_{geo,PW}$ in $s^{-1}$ | 6.73 | 8.01 | 8.89 | 10.75 |

### 3.1.3 | Mass transfer measurements

Mass transfer measurements in the test facility described in Section 2.3 complete the characterization of the initial structure RP9M-3D. Figure 8A shows the height of a transfer unit $HTU_{OG}$ as a function of the *F*-factor for the RP9M-3D at DN50 and DN20. The uncertainty analysis is explained in the Supporting Information.

Each plot corresponds to a series of measurements between which the columns were completely disassembled and reassembled to investigate reproducibility. At DN50 at low *F*-factors, a large scattering of the measurement results is observed, which disappears as the gas load increases. Accordingly, reproducibility is impaired, especially at low gas loads. The measurement series themselves were always measured twice. For illustrative reasons, only one plot is shown for each measurement series. Since the results were nearly identical, a high repeatability could be concluded.[25]

In general, there is a decreasing trend in separation efficiency (increasing $HTU_{OG}$-values) with increasing gas loads for DN50 and DN20. Contrary to the expectations of the single-phase gas flow simulations, the separation performance of DN50 and DN20 is very similar, although the latter has a much higher surface area $a_{geo,PW}$ due to the larger wall fraction. Miniaturized columns tend to cause stronger deflection of the liquid flow toward the column wall. In this case, the liquid can flow unhinderedly downwards over large regions of the wall, so that an uneven liquid flow velocity profile develops in the column. It is common knowledge that wall flow is detrimental to separation efficiency and scalability.[39] Since this effect increases with diameter reduction, the positive influence of the extra wall area on the $HTU_{OG}$-value is neutralized. Such behavior cannot be captured by the single-phase gas flow simulation, though. Based on the characterization of the RP9M-3D presented in this section, a clear potential for improvement can be noted.

Steude et al.[40] show results of mass transfer measurements for the original RP9M with the substance system chlorobenzene/ethylbenzene. Although no column diameter is given for the measurements, it is assumed that the diameter was larger than DN20 and thus only the DN50 measurement data can be directly compared. In this case, the same trend of a decreasing separation efficiency with increasing gas loads can be observed, as for the RP9M-3D. However, the separation efficiency in the additively manufactured structure is lower, presumably due to the usage of a different test system and because no wall wipers were integrated. Furthermore, the 3D-printed version is not completely identical to the original Rombopak 9M in terms of its dimensions.

## 3.2 | Packing modification: A new packing structure

Based on the characteristic features of the RP9M-3D, initial hypotheses are postulated in this section, which are used for the development of a new packing with improved properties. For this purpose, the various advantages and disadvantages of the RP9M-3D are briefly summarized.

On the one hand, the original RP9M is known for its relatively good scalability properties. This can also be observed for the RP9M-3D, however, with an overall lower separation efficiency.[40] Although there is a trend of decreasing separation efficiency with increasing *F*-factor in the considered region, it is not exceedingly pronounced. The main problem for scalability is the high scatter of results at low *F*-factors. In addition, an even flatter $HTU_{OG}$-curve at higher separation efficiencies is desired. To improve the RP9M-3D for scale-up purposes, two design changes are incorporated into a new advanced packing structure. These changes are hypothesized as the cause of potential improvement and are as follows:

1. Inhomogeneities and anisotropies in packings have to be eliminated as far as possible.
2. Shortcut flows of the gas and liquid phase must be reduced to a minimum.

Figure 4 illustrates the new packing structure, hereafter referred to as XW-Pak. Based on the X-shaped unit cell (A), a cuboid packing layer (B) is created. A cylinder is cut out of this (C). A mirrored cylindrical layer rotated by 90° (D) is then stacked to fit the cylindrical layer below. The desired packing height can be reached by stacking the repetition unit consisting of two cylindrical layers (C) and (D).

In this packing structure, unlike the RP9M-3D (Figure S1), inhomogeneities do not occur when stacking multiple packing layers. The two packing layers can be rotated by 90° to each other without forming inhomogeneities when stacking different packing segments. Anisotropic regions at the intersections of packing and column wall do not exist in the structures presented hereafter, since they are additively manufactured to fit precisely. In addition, shortcut flows (fluid bypasses) are prevented by the fact that a cylindrical layer fills the entire cross-section when the packing is viewed from above, as illustrated in Figure 5B. Figure 5A shows the top view of a packing segment of the RP9M-3D. These are 9 cm high and need to be rotated by 90° to the adjacent segments. This closes the gaps in the top view a little further, but only in an 9 cm interval. With the XW-Pak, this happens from packing layer to packing layer every 2.5 cm. Furthermore, the cross-section of a single packing layer of the XW-Pak is almost completely closed when viewed from above.

As a result, liquid at the wall cannot flow downwards unhinderedly at high velocities and thereby bypass the inner structure. Although this effect could be minimized by installing wall wipers, the feasibility of doing so is questionable for the target diameter of DN20 as this leads to an abrupt reduction of the cross-section and thus to higher flow resistance and pressure drop. In addition, wall wipers represent a new inhomogeneity in the packing structure (wall wipers together with a wall gap).

Furthermore, both the gas and the liquid phase are much better mixed, as illustrated in Figure 6 for the liquid phase. Figure 6A illustrates a DN20 repetition unit of the XW-Pak that is used for the two-phase flow simulation of the irrigation behavior (compare Section 2.2.2). Once the simulation is started, the packing is irrigated with *n*-heptane. Figure 6B shows a packing section in the initial phase

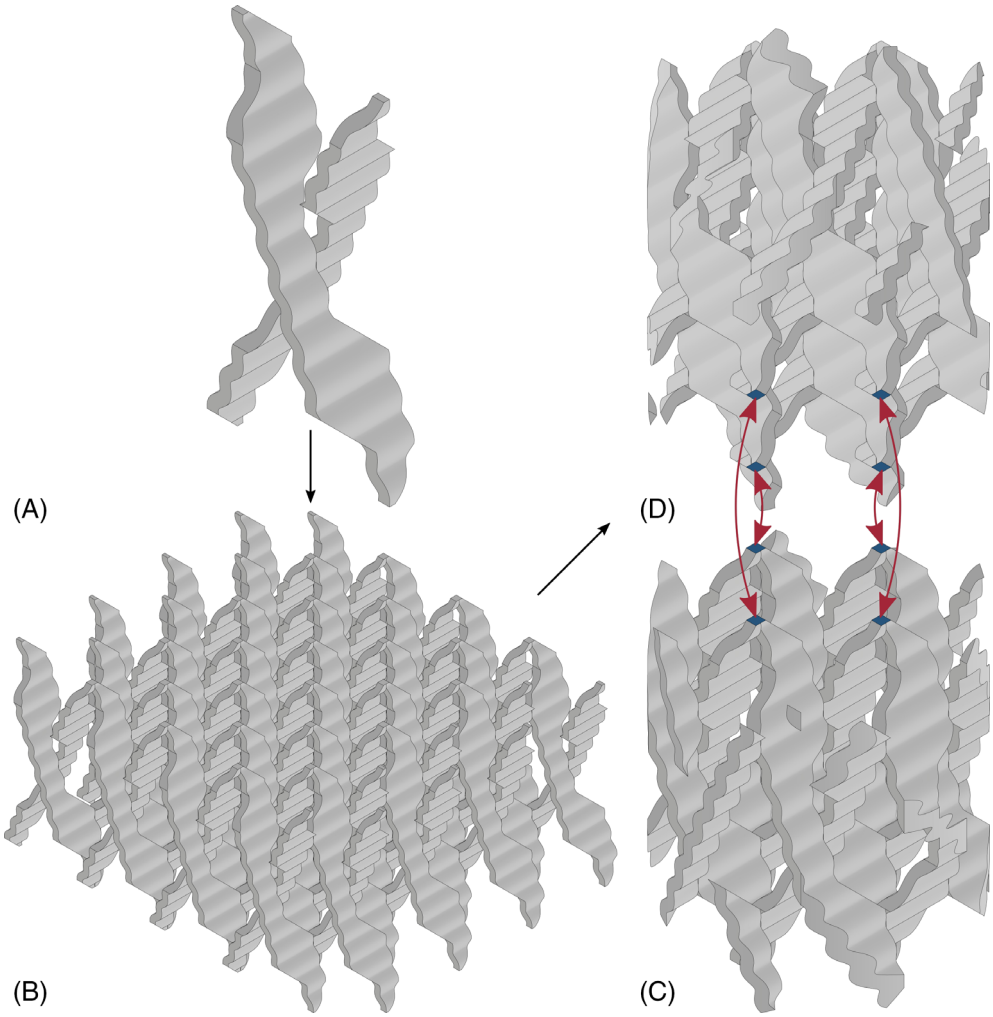


**FIGURE 4** Design properties of the new XW-Pak structure, (A) Unit cell, (B) Cuboid packing layer, (C) Cylindrical packing layer and (D) Cylindrical packing layer, rotated by 90° and mirrored

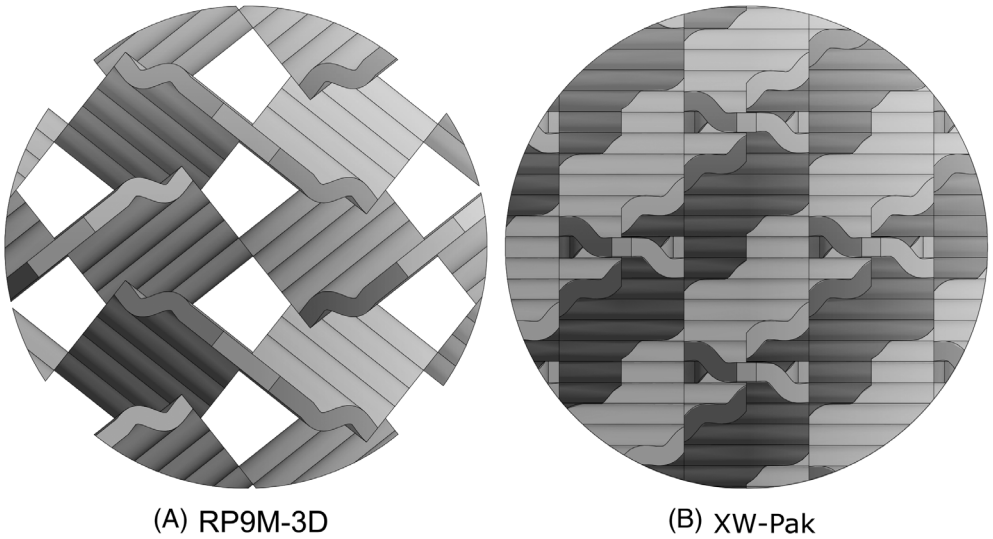


**FIGURE 5** Top view of the RP9M-3D (A) and the XW-Pak (B)

of the simulation, while Figure 6C describes a state shortly after the drop impact. At the junction of the packing layers, the liquid can converge at one point. As it flows down, it is redistributed on the associated crosspieces. The gas flow is also directed to this point and distributed radially in the layer above. These spots contribute to better mixing, cross-distribution, and renewal of the liquid film.

For the new packing structure, a design of experiment was performed for the single-phase gas flow simulations in order to

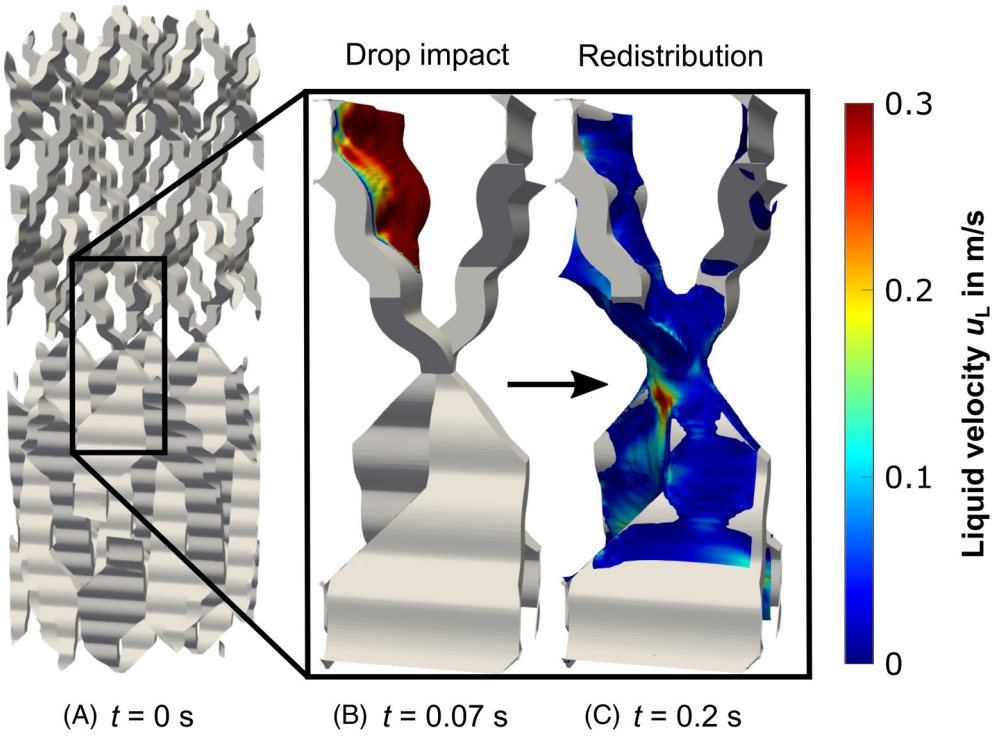


**FIGURE 6** Liquid redistribution after drop impact at the packing layer intersections

find an optimal design. These were followed by the much more time-consuming two-phase flow simulations of the irrigation behavior. In this work, a version of the XW-Pak with almost identical geometric characteristic properties as the RP9M-3D is presented to allow a fair comparison of the two structures. The geometric properties of the RP9M-3D and the XW-Pak are listed in Table 1.

## 3.3 | Characterization of the XW-Pak

The same tools as for the RP9M-3D are used to characterize the XW-Pak. Sections 3.3.1 and 3.3.2 present the results of the single-phase gas flow and the two-phase flow simulations. Final conclusions, on whether the evolution of RP9M-3D towards XW-Pak is an improvement or not, are discussed in terms of the experimental results shown in Section 3.3.3.

### 3.3.1 | Single-phase gas flow simulation

For the XW-Pak, the single-phase gas flow simulations are performed to determine the specific dry pressure drop $\Delta p_d/H_P$ and (volumetric) mass transfer coefficients $\beta$ and $\beta \cdot a_{geo,PW}$. The results are shown in Table 2 and compared to the RP9M-3D results. The general trends and observations derived from the single-phase gas flow simulations were discussed in Section 3.1.1 for the RP9M-3D. These remain the same for the XW-Pak. Nevertheless, there are significant differences in the values. The pressure drop increases by 9.7% when reducing the column diameter to DN20.

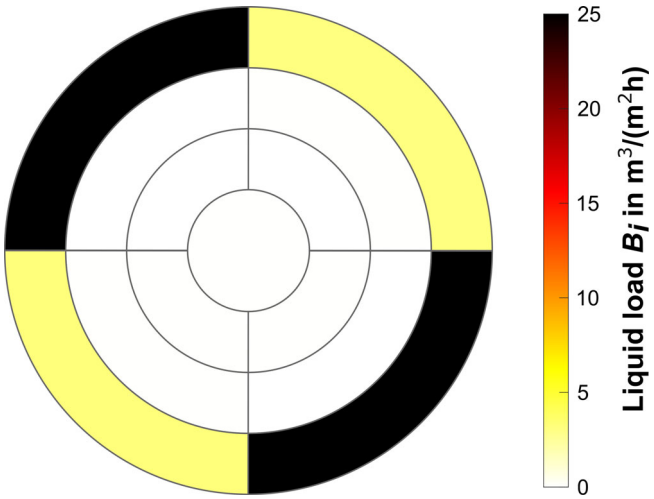


**FIGURE 7** Simulated liquid distribution at the domain ends of the XW-Pak with an overall liquid load of $B = 6.8$ m$^3$ m$^{-2}$ h$^{-1}$ at DN20 (according to Sarajlic et al.[36])

As for the RP9M-3D, the mass transfer coefficient $\beta$ decreases slightly at DN20 (compare Section 3.1.1). When analyzing the mass transfer efficiency, the volumetric mass transfer coefficient $\beta \cdot a_{geo,PW}$ increases by 21.0% for the DN20 simulation compared to DN50.

When directly comparing the results of the single-phase gas flow simulations of RP9M-3D and XW-Pak, a significantly higher specific dry pressure drop is obtained for the latter. At DN50 this value is increased by 62.9% and at DN20 by 58.8%. An absolute value of 2 mbar/m was defined as the maximum value, which is still met by the XW-Pak.

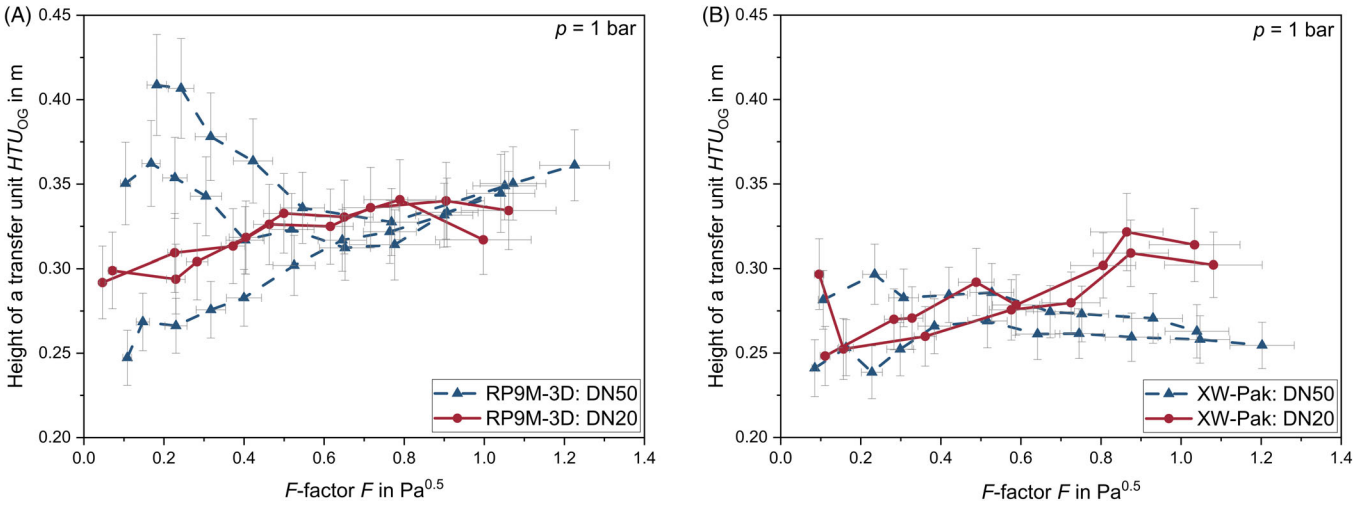


**FIGURE 8** Separation efficiency at different *F*-factors in DN50 and DN20. (A) RP9M-3D and (B) XW-Pak

Further investigations show that radial mixing inside the XW-Pak structure increases significantly. For this purpose, the average radial velocity $u_{rad}$ was calculated in the packing region according to Equation (7) with the average velocity fractions in *x* and *y* direction $u_x$ and $u_y$. An increase in the radial velocity of approximately 25% was observed for the XW-Pak structure, indicating a better radial gas-phase mixing which can justify the improved mass transfer.

$$u_{rad} = \left(u_x^2 + u_y^2\right)^{0.5} \tag{7}$$

Because of the considerably increased homogeneity of the XW-Pak as a result of improved radial mixing, the finer structure, and the avoidance of shortcut flows, the volumetric mass transfer coefficients $\beta \cdot a_{geo,PW}$ of the XW-Pak increase by 32.2% for DN50 and 34.3% for DN20. Based on the single-phase gas flow simulations, a significant increase in separation efficiency can be expected in the experiments. First, however, two-phase flow simulations of the irrigation behavior must be performed to allow a more reliable prediction.

### 3.3.2 | Two-phase flow simulation of the irrigation behavior

The results of the characterization of the XW-Pak by two-phase flow simulations of the irrigation behavior can be found in a previous publication.[36] In addition, the liquid distribution is illustrated in Figure 7. The liquid distribution at DN20 of the XW-Pak shows an increased wall flow in two opposite wall segments, illustrated in black. This effect also occurs with the RP9M-3D, but to a lesser extent. In addition, there is only a very small fluid flow in the interior segments of the structure. The improvement in separation efficiency predicted by the single-phase gas flow simulation is expected to be lower due to the results from the two-phase flow simulation. This is confirmed by experimental measurements of the XW-Pak.

### 3.3.3 | Mass transfer measurements

Figure 8B shows the height of a transfer unit $HTU_{OG}$ across the *F*-factor for the XW-Pak at DN50 and DN20. The uncertainty analysis is explained in the Supporting Information. Again, a plot corresponds to a series of measurements. Each series was measured twice. For clarity, however, only one representative plot is shown. For the generation of each plot, the columns were completely disassembled and reassembled. With the RP9M-3D, strong variances of the measurement results became noticeable in the low *F*-factor range. These scattering effects were significantly reduced with the XW-Pak. At DN50, there is an almost constant course of the separation efficiency, which means that high scalability can be assumed. Unfortunately, when the diameter was reduced to DN20, a slight slope of the separation efficiency curve reappears. In general, however, an increased overall separation efficiency of the XW-Pak can be detected when comparing it to the RP9M-3D. Based on this finding, a third hypothesis is formulated for the improvement of packing structures for scale-up applications.

3. Liquid wall flow must be reduced to a reasonable extent. This does not mean that liquid wall flow in general is detrimental.

To estimate a reasonable extent of the liquid mass flow $\dot{m}_W$ at the wall to the mass flow $\dot{m}_P$in the packing, the ratio of the geometric surface $a_{geo,W}$ of the wall to the geometric packing surface $a_{geo,P}$ can be used, as shown in Equation (8).

$$\frac{\dot{m}_W}{\dot{m}_P} = \frac{a_{geo,W}}{a_{geo,P}} \tag{8}$$

For the relative packing improvement (*RPI*) regarding the mass transfer in the experiment (Exp), the $HTU_{OG}$-values of the XW-Pak are related to those of the RP9M-3D at the same *F*-factor $F \approx 1.0$ Pa$^{0.5}$ according to the left side of Equation (9). Taking into account the simplifications of the single-phase gas flow simulations, the CFD

predicted $RPI_{CFD}$ can be calculated according to the right side of Equation (9), since gas velocities, cross-sectional area, and diameter are identical. The same *F*-factors $F = 1.0\ \mathrm{Pa}^{0.5}$ are used for direct comparison with the experimentally determined $RPI_{Exp}$ value.

$$RPI_{Exp} = 1 - \frac{HTU_{OG}^{XW\text{-}Pak}}{HTU_{OG}^{RP9M\text{-}3D}} \quad \text{and} \quad RPI_{CFD} = 1 - \frac{\beta^{RP9M\text{-}3D} \cdot a_{geo,PW}^{RP9M\text{-}3D}}{\beta^{XW\text{-}Pak} \cdot a_{geo,PW}^{XW\text{-}Pak}} \tag{9}$$

For DN50 the $RPI_{Exp}$-value was 25.1% and for DN20 5.9%. The CFD-predicted $RPI_{CFD}$-value according to the single-phase gas flow simulation was 24.3% for DN50 and 25.5% for DN20. For DN50, a very good agreement between CFD and experiment is observed. Finally, the validity of the assumption that both packings are similarly wetted is reassessed by including the two-phase liquid flow simulations of the irrigation behavior.

Since liquid distribution significantly deteriorates at reduced diameter as a result of wall flow, the difference in $RPI_{Exp}$- and $RPI_{CFD}$-values at DN20 can be explained. Since wall flow is more pronounced in the XW-Pak than in the RP9M-3D, the approx. 25.5% improvement in separation efficiency at DN20 as predicted by the single-phase gas flow simulations were overestimated by 19.6%. As a result, the prediction of the separation performance, especially of miniaturized columns, is done from a joint consideration of single-phase gas flow simulation and two-phase flow simulations of the irrigation behavior.

## 4 | SUMMARY AND OUTLOOK

Within this publication, a methodology is presented that can be used to systematically develop enhanced packings based on an initial structure. So far, no systematic approach for the development of laboratory scale packings exists that considers fluid dynamic and mass transfer properties in the packing design. In the context of a successful case study, the methodology is applied to generate miniaturized scalable packings that exhibit a constant separation efficiency independent of the gas load. Individual tools of this methodology have already been addressed in other publications. In this article, the entire workflow is presented and it is demonstrated that the approach works.

The introduced procedure is characterized by an iterative approach and an interplay between design, CFD, 3D printing, and experimental investigations. The creation of packing structures with the CAD software Autodesk Inventor® is largely automated using the VBA interface together with fully parameterized packing structures. Single-phase gas flow simulations and simulations of the liquid flow distribution allow for an early characterization of different packing designs. Promising structures are 3D printed and examined in a distillation test rig that can be operated with column diameters DN50 to DN20. The objective of the joint research project between the Ulm University, the Technical University of Munich, and BASF SE is to create miniaturized, scalable packed columns for distillation. For the target diameter DN20, a high separation efficiency independent of the *F*-factor is the objective. Based on the findings of the characterization of the initial structure, two hypotheses on how to improve packing structures in terms of scalability behavior were formulated. On the one hand, (1) inhomogeneities and anisotropies in packings have to be eliminated as far as possible. On the other hand, (2) shortcut flows of the gas and liquid phase must be reduced to a minimum. Thereby, an advanced packing structure (XW-Pak) was created. At DN50, *F*-factor independent $HTU_{OG}$-values and an increase in the overall separation efficiency, compared to the initial structure, could already be recorded.

At DN20, wall effects dominate, which leads to an equalization of the separation properties of both packings. Therefore, a third hypothesis for the improvement of the scalability properties was derived, stating that (3) the liquid wall flow must be reduced to a reasonable extent.

It was possible to significantly improve the initial RP9M-3D structure. The XW-Pak represents an intermediate step in the development and proves that the methodology works. This emphasizes the promising approach to improving packing structures.

Future work focuses on the continuous development of packing structures for scale-up applications. To further improve scalability, a new insulation concept specifically for miniaturized column systems is under development. The objective is the reduction of heat losses across the column wall, preventing unwanted condensation and allowing accurate measurements of fluid flows within the column. Furthermore, the intentionally simple simulation approaches are to be further developed in such a way that the validity is increased while the computational effort remains the same. Gas–liquid flows in packing structures under consideration of mass transfer inevitably lead to disproportionately large computation times. This would not be practicable within the methodology. Consequently, approaches are pursued in which results and findings from the simulation of the liquid flow distribution are used as input for the single-phase gas flow simulation to maintain the easy and robust simulation characteristics.

### LATIN SYMBOLS

| | |
|---|---|
| $A$ | area, $\mathrm{m}^2$ |
| $a$ | specific area, $\mathrm{m}^2\ \mathrm{m}^{-3}$ |
| $B$ | liquid load, $\mathrm{m}^3\ \mathrm{m}^{-2}\ \mathrm{h}^{-1}$ |
| $c$ | concentration, $\mathrm{mol}\ \mathrm{m}^{-3}$ |
| $D$ | diffusion coefficient, $\mathrm{m}^2\ \mathrm{s}^{-1}$ |
| $d$ | diameter, m |
| $F$ | *F*-factor, $\mathrm{Pa}^{0.5}$ |
| $H$ | height, m |
| $h$ | enthalpy, m |
| $HETP$ | height equivalent to a theoretical plate, m |
| $HTU$ | height of a transfer unit, m |
| $L$ | length, m |
| $\dot{N}$ | molar flow, $\mathrm{mol}\ \mathrm{s}^{-1}$ |
| $p$ | pressure, Pa |
| $RPI$ | relative packing improvement, % |
| $T$ | temperature, K |
| $t$ | time, s |
| $u$ | velocity, $\mathrm{m}\ \mathrm{s}^{-1}$ |
| $\dot{V}$ | volume flow, $\mathrm{m}^3\ \mathrm{s}^{-1}$ |
| $x$ | molar fraction, $\mathrm{mol}\ \mathrm{mol}^{-1}$ |

## GREEK SYMBOLS

| | |
|---|---|
| $\alpha$ | relative volatility |
| $\beta$ | mass transfer coefficient, $m^3\ m^{-2}\ s^{-1}$ |
| $\varepsilon$ | void fraction, % |
| $\lambda$ | stripping factors |

## SUBSCRIPTS AND SUPERSCRIPTS

| | |
|---|---|
| 1 | low-boiling component |
| 2 | high-boiling component |
| avg | average |
| B | bottom |
| C | column |
| CFD | CFD-simulation |
| d | dry |
| Exp | experiment |
| G | gas |
| geo | geometric |
| L | liquid |
| log | logarithmic |
| OG | overall gas |
| P | packing |
| PW | packing with column wall |
| T | top |
| V | evaporation |

## NOTATION

| | |
|---|---|
| CAD | computer-aided design |
| CFD | computational fluid dynamics |
| PA12 | polyamide 12 |
| SLS | selective laser sintering |
| RP9M | Rombopak 9M |
| RP9M-3D | 3D printable version of the Rombopak 9M |
| VBA | visual basic for applications |

## AUTHOR CONTRIBUTIONS

**Johannes Neukäufer:** Conceptualization (lead); data curation (lead); formal analysis (lead); investigation (lead); methodology (equal); validation (lead); visualization (lead); writing – original draft (lead); writing – review and editing (lead). **Mohamed Adel Ashour:** Conceptualization (supporting); formal analysis (supporting); investigation (supporting); methodology (equal); validation (supporting); writing – review and editing (equal). **Nadin Sarajlic:** Conceptualization (supporting); investigation (supporting); methodology (equal); writing – review and editing (equal). **Harald Klein:** Funding acquisition (equal); methodology (supporting); supervision (supporting). **Sebastian Rehfeldt:** Funding acquisition (equal); methodology (equal); project administration (equal); supervision (equal); writing – review and editing (equal). **Heiko Hallmann:** Conceptualization (supporting). **Sebastian Meinicke:** Conceptualization (supporting); methodology (equal); writing – review and editing (equal). **Jürgen Paschold:** Conceptualization (supporting); investigation (supporting); methodology (equal). **Carsten Knösche:** Conceptualization (supporting); investigation (supporting); methodology (equal); project administration (lead); writing – review and editing (equal). **Thomas Grützner:** Conceptualization (supporting); funding acquisition (lead); methodology (equal); project administration (equal); resources (lead); supervision (lead); writing – review and editing (equal).

## ACKNOWLEDGMENT

Open Access funding enabled and organized by Projekt DEAL.

## DATA AVAILABILITY STATEMENT

The data that support the findings of this study are available from the corresponding author upon reasonable request.

## ORCID

*Johannes Neukäufer* https://orcid.org/0000-0003-1115-9503
*Nadin Sarajlic* https://orcid.org/0000-0002-0923-8045

## REFERENCES

1. Gładyszewski K, Skiborowski M. Additive manufacturing of packings for rotating packed beds. *Chem Eng Process: Process Intensif*. 2018;127:1-9.
2. Wen Z-N, Wu W, Luo Y, Zhang L-L, Sun B-C, Chu G-W. Novel wire mesh packing with controllable cross-sectional area in a rotating packed bed: mass transfer studies. *Ind Eng Chem Res*. 2020;59(36):16043-16051.
3. Qammar H, Gładyszewski K, Górak A, Skiborowski M. Towards the development of advanced packing design for distillation in rotating packed beds. *Chem Ing Tech*. 2019;91(11):1663-1673.
4. Bara JE, Hawkins CI, Neuberger DT, Poppell SW. 3D printing for $CO_2$ capture and chemical engineering design. *Nano Energy*. 2013;2(5):235-243.
5. Bolton S, Kasturi A, Palko S, et al. 3D printed structures for optimized carbon capture technology in packed bed columns. *Sep Sci Technol*. 2019;54(13):2047-2058.
6. Miramontes E, Love LJ, Lai C, Sun X, Tsouris C. Additively manufactured packed bed device for process intensification of $CO_2$ absorption and other chemical processes. *Chem Eng J*. 2020;388:124092.
7. Xiao M, Sarma M, Thompson J, Nguyen D, Ruelas S, Liu K. $CO_2$ absorption intensification using three-dimensional printed dynamic polarity packing in a bench-scale integrated $CO_2$ capture system. *AIChE J*. 2022;68(4):e17570.
8. Grinschek F, Xie D, Klumpp M, Kraut M, Hansjosten E, Dittmeyer R. Regular microstructured elements for intensification of gas–liquid contacting made by selective laser melting. *Ind Eng Chem Res*. 2020;59(9):3736-3743.
9. Dejean B, Meyer M, Rouzineau D. Design and conception of an innovative packing for separation column—part I: hydrodynamic study on wire intersections. *Chem Eng Res Des*. 2020;160:11-19.
10. Zimmer A, PachecoAraújo JD, Andreassen KA, Grande CA. Effect of manufacturing techniques in pressure drop on triple periodical minimal surface packings. *Chem Ing Tech*. 2021;93:967-973.
11. Reitze A, Grünewald M, Riese J. Characterization of liquid-phase distribution in 3D printed structured Packings with an enclosed Column Wall. *Ind Eng Chem Res*. 2022;61(1):740-746.
12. Riese J, Reitze A, Grünewald M. Experimental characterization of 3D printed structured metal packing with an enclosed column wall. *Chem Ing Tech*. 2022;94:993-1001.
13. Mardani S, Ojala LS, Uusi-Kyyny P, Alopaeus V. Development of a unique modular distillation column using 3D printing. *Chem Eng Process: Process Intensif*. 2016;109:136-148.
14. Grinschek F, Dübal S, Klahn C, Dittmeyer R. Einfluss des additiven fertigungsverfahrens auf die gestalt einer mikrorektifikationsapparatur. *Chem Ing Tech*. 2022;94:958-966.
15. Sholl DS, Lively RP. Seven chemical separations to change the world. *Nature*. 2016;532(7600):435-437.

16. Stichlmair J, Klein H, Rehfeldt S. *Distillation: Principles and Practice (2nd Edition)*. Wiley-AIChE; 2021.
17. Fent K. *Ökotoxikologie: Umweltchemie, Toxikologie, Ökologie*. 4th ed. Thieme; 2013.
18. Grossman E. *Chasing Molecules: Poisonous Products, Human Health, and the Promise of Green Chemistry*. Island Press; 2009.
19. United States Government Accountability Office. *Toxic Substances: EPA has Increased Efforts to Assess and Control Chemicals but Could Strengthen its Approach: Report to Congressional Requesters*. United States Government Accountability Office; 2017.
20. Hufton JR, Bravo JL, Fair JR. Scale-up of laboratory data for distillation columns containing corrugated metal-type structured packing. *Ind Eng Chem Res*. 1988;27(11):2096-2100.
21. Eiden U, Kaiser R, Schuch G, Wolf D. Scale-up von Destillationskolonnen. *Chem Ing Tech*. 1995;67(3):269-279.
22. Onken U. *Recommended Test Mixtures for Distillation Columns*. 2nd ed. The Institution of Chemical Engineers; 1990.
23. Schoenmakers H, Spiegel L. Laboratory distillation and scale-up. In: Gorak A, ed. *Distillation: Equipment and processes*. Elsevier Science; 2014:319-339.
24. Neukäufer J, Hanusch F, Kutscherauer M, Rehfeldt S, Klein H, Grützner T. Methodology for the development of additively manufactured packings in thermal separation technology. *Chem Eng Technol*. 2019;42(9):1970-1977.
25. Neukäufer J, Sarajlic N, Klein H, et al. Flexible distillation test rig on a laboratory scale for characterization of additively manufactured packings. *AIChE J*. 2021;67(11):e17381.
26. Bühlmann, Ulrich, Kühni AG. *Packing for material exchange columns*. US Patent 4501707; July 07, 1982.
27. Sacher J, Repke J-U. Development of a mesoscale model for the gas phase fluid dynamics in structured packings based on fundamental experiments and CFD investigations. *Chem Eng Res Des*. 2019;147:430-442.
28. Stephan P, Kabelac S, Kind M, Mewes D, Schaber K, Wetzel T, eds. *VDI-Wärmeatlas: Mit 1046 Abbildungen und 483 Tabellen*. 12th ed. Berlin, Heidelberg; 2019.
29. de Lemos M. *Turbulence in Porous Media: Modeling and Applications*. 2nd ed. Elsevier; 2012.
30. Amini Y, Karimi-Sabet J, Esfahany MN. Experimental and numerical simulation of dry pressure drop in high-capacity structured packings. *Chem Eng Technol*. 2016;39(6):1161-1170.
31. Macfarlan LH, Phan MT, Eldridge RB. Methodologies for predicting the mass transfer performance of structured packings with computational fluid dynamics: a review. *Chem Eng Process: Process Intensif*. 2022;172:108798.
32. Poling BE, Prausnitz JM, O'Connell JP. *The Properties of Gases and Liquids*. 5th ed. McGraw-Hill; 2001.
33. Tominaga Y, Stathopoulos T. Turbulent Schmidt numbers for CFD analysis with various types of flowfield. *Atmos Environ*. 2007;41(37):8091-8099.
34. Macfarlan LH, Seibert AF, Phan MT, Eldridge RB. CFD-based study on structured packing geometry. *Chem Eng Sci*. 2021;243:116767.
35. Seader JD, Henley EJ, Roper DK. *Separation Process Principles*. 3rd ed. Wiley; 2011.
36. Sarajlic N, Neukäufer J, Ashour M, et al. Simulation of the liquid flow distribution in laboratory-scale additively manufactured packings. *Authorea*. 2022.
37. Neukäufer J, Seyfang B, Grützner T. Investigation of contact angles and surface morphology of 3D-printed materials. *Ind Eng Chem Res*. 2020;59(14):6761-6766.
38. Čmelíková T, Valenz L, Lyko Vachková E, Rejl FJ. Basic separation efficiency and hydraulic data of MellapakPlus 452.Y structured packing under distillation conditions. *Chem Eng Res Des*. 2021;172:175-185.
39. Deibele L, Dohrn R. *Miniplant-Technik in der Prozessindustrie*. 1st ed. Wiley-VCH; 2006.
40. Steude HE, Deibele L, Schröter J. MINIPLANT-Technik-ausgewählte Aspekte der apparativen Gestaltung. *Chem Ing Tech*. 1997;69(5):623-631.

## SUPPORTING INFORMATION

Additional supporting information can be found online in the Supporting Information section at the end of this article.

**How to cite this article:** Neukäufer J, Ashour MA, Sarajlic N, et al. Development of enhanced three-dimensional printed packings for scale-up of distillation columns: A successful case study. *AIChE J*. 2023;69(3):e17902. doi:10.1002/aic.17902